FORMATION OF DENSE SILICON CARBIDE BY MOLTEN SILICON INFILTRATION OF CARBON WITH TUNED STRUCTURE

Jesse C. Margiotta, Department of Materials Science and Engineering, The Johns Hopkins University, Baltimore, MD 21211
Dajie Zhang, Advanced Technology Laboratory, The Johns Hopkins University, Baltimore, MD 21211
Dennis C. Nagle, Advanced Technology Laboratory, The Johns Hopkins University, Baltimore, MD 21211

Abstract

Carbon preforms are being developed from cellulose-based precursors for the formation of fully dense SiC monoliths by a liquid phase Si infiltration technique. The carbon structural characteristics such as bulk density, microporosity and solid reactivity are paramount in determining the effectiveness of the SiC formation process. To adjust the carbon structural properties thus allowing successful liquid Si infiltration and SiC formation, a precursor composite of cellulose and phenolic resin was created. For the carbonization process, researchers adopted a hybrid procedure of low-temperature oxidative curing in air atmosphere followed by high-temperature carbonization in argon to obtain carbons with desired bulk densities and macroporosities. In the SiC formation process, carbon disks were embedded in fine Si powder inside graphite crucibles. These crucibles were then placed in a high-temperature graphite vacuum furnace at a temperature of 1800ºC and pressures of about 0.5 Torr for various time lengths. After studying the samples produced by this process, researchers discovered that SiC disks with apparent densities of greater than 91 percent of that of pure SiC can be achieved with just one infiltration cycle from a precursor composite of 6:4 mass ratio of cellulose to phenolic resin. The successful SiC conversion this material exhibits is attributable to the high reactivity of the cellulose-derived phase and the structural rigidity and low reactivity of the phenolic phase combined with a narrow pore size distribution above 1 μm. The reaction mechanism of this process is believed to be dissolution of carbon by molten Si followed by the nucleation and growth of SiC microcrystallites.

Introduction

The conversion of porous carbon structures by liquid silicon infiltration techniques to silicon carbide has been extensively studied[1,3-5,9,11]. Zhou and Singh and Favre, Fuzellier and Suptil[6,12] have shown that liquid silicon metal conversion of glass carbon to silicon carbide results in the formation of a dense thin 10 micron layer of carbide on the glassy carbon that creates a diffusion barrier preventing further reaction. Glass carbon which is made from pure phenolic resin has a dense microporous structure (pore diameters less than 2 nm) with little open macroporosity (pore diameters greater than 50 nm) to allow penetration of the liquid metal into the carbon structure, and thus, this material is highly resistant to bulk carbide formation. Conversely, studies by Kercher and Nagle demonstrated the ability to completely convert carbonized medium density fiber board and masonite materials to silicon carbide; however, these materials produced silicon carbide with densities in only in the 80 to 90% range.

The focus of the study has been to engineer carbon monolithic structures with bulk densities, macroporosities and reactivities that will allow liquid silicon to fully infiltrate the carbon structure to consistently form high density silicon carbide as depicted in Figure 1. As a model system, microcrystalline cellulose bonded with phenolic resin was selected to introduce an open porosity into the glassy carbon to allow liquid metal infiltration. These two materials were selected for this study because they were readily available, have been well characterized, are available commercial materials and because they are essentially free of impurities that can alter both the carbonization and carbide formation process. In addition, these two materials behave very differently upon carbonization. Phenolic resin shrinks much less that cellulose on carbonization, has much less microporosity which are mostly closed and has a carbon yield of about 64% compared to cellulose which yields about 9%. Phenolic resin has a dimensional yield of about 82% while crystalline cellulose yields 51% of its original dimensions.

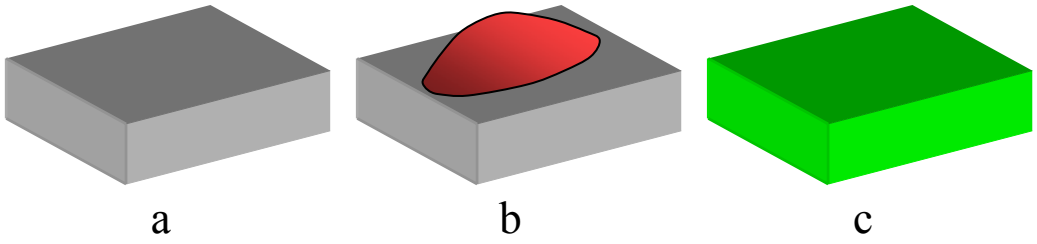

Figure 1. Formation of SiC by molten silicon infiltration of porous carbon occurs when a porous carbon machined to desired geometry **(a)** is introduced to liquid-phase silicon **(b)**. The reduction in surface energies of both the molten silicon and solid carbon leads to reactive wetting and wicking of porous solid carbon by molten silicon and the free energy reduction associated with the highly exothermic reaction leads to the formation of the reaction product, SiC **(c)**. It is of special significance that the macrostructure, or geometry, of the initial porous carbon is retained during the siliconization process.

Tuning Carbon Bulk Density, Macroporosity and Reactivity

Carbon structure, from macroporosity to atomic ordering, is of key importance in determining the effectiveness of the siliconization process. Of the many carbon structural properties, three are of great significance:

1. Bulk density
2. Macroporosity
3. Carbon reactivity

Carbon bulk density, ρ_B, and pore diameter, d_P, have been examined before[1,3,9,11] but solid carbon reactivity has not.

The bulk density of the porous carbon, ρ_B, is the mass per unit volume including both solid and voids. A porous carbon with the ideal bulk density will allow fully dense homogeneous SiC formation and is obtained by considering that the number of moles of carbon per unit volume must remain the same in SiC and the porous carbon precursor

$$\rho_B = \frac{M_C}{V_{SiC}} = \frac{\rho_{SiC} M_C}{M_{SiC}} = 0.964 \, {}^{g}\!/_{cm^3}$$

where M_C and M_{SiC} are the molar masses of carbon and SiC, V_{SiC} is the molar volume of SiC and ρ_{SiC} is the density of SiC. If the carbon bulk density is below the ideal value there will not be enough carbon per unit volume to allow homogenous SiC formation; when all of the carbon is consumed excess silicon will remain and a composite of SiC and silicon will result. If the carbon bulk density is above the ideal value, once the pores have filled with silicon there will not be enough silicon per unit volume for homogenous SiC formation; when all of the silicon is consumed excess carbon will remain and a composite of SiC and carbon will result.

The importance of macroporosity has been shown to manifest itself in pore diameter, d_P. Darcy's law is an empirical relation stating that the infiltration velocity varies directly with the square of pore diameter

$$v = \frac{dh}{dt} = -\frac{\kappa}{\mu}\nabla p = -\frac{C d_P^2}{\mu}\nabla p$$

for which v is fluid velocity, h is the height in the pores of the fluid flow, μ is fluid viscosity, p is pressure, and κ is the permeability of the porous solid and C is dimensionless constant. For the case of bulk siliconization it is better for infiltration to happen as quickly as possible to allow reaction to occur through the entire sample simultaneously. Because of this and the liquids velocity dependence on the square of d_P

the pore diameter should be maximized. Another concern is that pores below a critical value have been shown to prevent effective siliconization due to pore closure resulting from the change in volume[1,3,9,11], ΔV, associated with carbon transformation to SiC which varies linearly with the carbon skeletal density, $\rho_{skeletal}$, according to the following simple relation:

$$\Delta V = V_{SiC} - V_C = \frac{M_{SiC}}{\rho_{SiC}} \frac{\rho_{skeletal}}{M_C} - 1 .$$

The carbon skeletal density can vary between 1.4 and 2.23 g cm^{-3} as the carbon structure changes from highly amorphous and microporous to graphitic so the change in volume can take values from 47.8 to 135.48 %. This volume increase leads to a reduction in the pore diameter as the reaction proceeds and has been shown to totally restrict further silicon flow for porous carbons with initial pore diameters less than approximately one micron and has been termed "pore-choking". Both pore-choking elimination and fluid velocity maximization are achieved by increasing diameter, however, it should be noted that increasing pore diameter can lead to an increase in porosity, (pore volume fraction) which reduces carbon bulk density. The bulk densities dependence on porosity and pore diameter can be found. Consider a solid enclosing a rectangular volume element of length, a, depth, b, and height, c, with cylindrical pores of a single diameter, d_P, extending vertically represented in Figure 2. The pore volume, V_P, the solid carbon volume, V_C and the bulk density are

$$V_P = \tfrac{1}{4}\pi d_P^2 cn ; \qquad V_C = V - V_P ; \qquad \rho_B = \frac{\rho_{skeletal} V_C}{V}$$

where c is the pore height, n is the pore concentration, V is the total volume and is the product of a, b and c. Rearranging leads to relationships between bulk density, porosity, pore diameter and skeletal density,

$$\rho_B = \frac{\rho_{skeletal}(V - V_P)}{V} = \rho_{skeletal}\left(1 - V_P/V\right) = \rho_{skeletal}\left(1 - \frac{\pi cn}{4V} d_P^2\right)$$

where V_P/V is equivalent to the porosity.

Carbon reactivity is directly related to the concentration and accessibility of 'active' sites within the solid. Active sites are imperfections in the solid structure such as unsatisfied valencies and irregular bond angles (kinks) which allow reaction with other species more readily. Active sites can be enclosed in a dense solid network thus eliminating possibility of exposure to reactant species. Conversely, many carbons have nanometer scale void networks rendering them highly reactive as their active sites are readily reached by reactant species. In Figure 2 the solid portion is itself microporous, having pores that are orders of magnitude smaller than the ones drawn. This solid contains within it both the active sites and microporous network. As a result, it is the skeletal density, including both solid and pores, that helps indicate reactivity. As the skeletal density decreases, the amount of microporosity and active sites increases and thus the solid reactivity increases. It is of note that the bulk density shares a one to one correlation with the skeletal density so as reactivity is increased, skeletal density and bulk density are decreased.

Our approach to tuning carbon bulk density, macroporosity and reactivity is to use various blends of particulate crystalline cellulose and phenol-formaldehyde (phenolic) resin as carbon precursors whose chemical structures are shown in Figure 3. Upon pyrolysis, crystalline cellulose leads to a carbon that is highly amorphous with little graphitic character present. Active sites at the

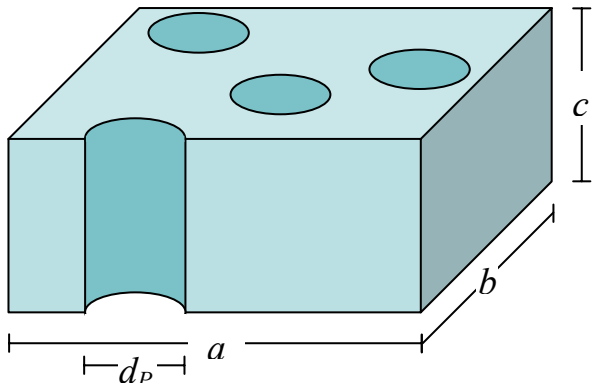

Figure 2. Schematic of porous carbon substrate of length, a, depth, b, height, c, and pore diameter d_P.

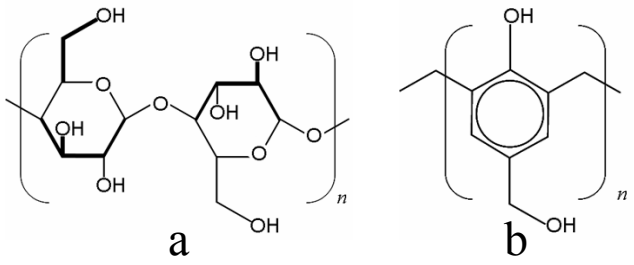

Figure 3. Chemical structures of crystalline cellulose (a) and phenolic resin (b).

edges of small atom clusters and at irregular bond kinks are plentiful. Additionally these carbons are highly microporous, having open pores in the range of 0.5-1 nm thus having high surface areas available to reaction and are considered highly reactive to molten silicon atoms. The macrostructure of substrates produced from crystalline cellulose particles is ruled by the particle packing of the original precursor as there is no glass transition and as a result is macroporous.

Phenolic resin yields a carbon that is also highly amorphous; however, the concentration of active sites is lower partly due to the hexagonal structure of the phenolic precursor. The micropores in this carbon are mostly closed and prevent easy travel for reactive species. Phenolic resin passes through a viscous phase during the pyrolysis procedure and when blended with crystalline cellulose particles it flows and can form a matrix within the structure. The carbon phase from each precursor is quite different and as a result the resulting carbon can be thought of as bimodal in structure.

Experimental Methods

Monolithic carbons of tuned porosity and reactivity were created from a precursor blend of crystalline cellulose (FMC Biopolymer, Avicel PH-105) and phenolic resin (Borden, Durite AD-5614). The precursors were blended in HDPE jars using alumina mixing media for 12 hours in mass fractions of phenolic resin of 0.1, 0.2, 0.25, 0.3, 0.35, 0.4, 0.45, 0.5, 0.6, 0.8 and 1.0. The precursor blends were cold-pressed in a 57 mm diameter cylindrical die under 35 MPa of pressure to 12 g cylindrical monoliths. The monolithic precursor blends were subjected to oxidative thermal treatment aimed to thermoset the phenol-formaldehyde resin phase and to oxidize the cellulose phase thus maximizing its weight loss and potential for microporosity. The treatment was done in an oven with air circulation fan (Applied Test Systems, Series 3710 Test Oven) using the thermal schedule in Table 1. The cured and thermally oxidized samples were carbonized in a high-temperature retort furnace (CM Rapid Temp, High Temperature Retort Furnace) with an inert argon flow of 0.5 mL min^{-1} using the thermal schedule in Table 1.

Siliconization experiments were performed in a water-cooled high-temperature graphite element vacuum furnace (Astro 1000A 4560 FP20 with a Eurotherm 2404 PID and type C thermocouple). Carbon monoliths were core drilled to 18 mm in diameter and packed in a bed of particulate silicon (Alfa Aesar, silicon powder, crystalline, -325 mesh, 99.5%) with a mass of that which would fully convert a mass 1.5 times that of the carbon sample to SiC. The reactor was a custom machined high-density graphite crucible with plug (GraphiteStore.com, 6cmOD 2.2cmID 6cmHIGH 4cmDEEP). The reactor was placed in the center of the furnace "hot zone" and a low pressure of near 0.5 Torr was maintained. The thermal schedule ensures sufficient outgas of graphite parts and the carbon sample. Additionally, an attempt to melt silicon as swiftly as possible is made to ensure that the carbon sample is in the presence of a uniform pool of molten silicon rather than small regions of molten silicon which can result in pitting of the sample. The thermal schedule is shown in Table 1.

Mass yields upon carbonization of the precursors were determined by simply dividing the pre-carbonization mass by the post-carbonization value. The carbon bulk density was determined for all blends by measuring the cylindrical dimensions. Pore characterization was performed by a mercury intrusion porosimeter (Micromeritics Poresizer 9320) yielding macropore size distribution, median macropore diameter, average macropore diameter, bulk density, skeletal density and macroporosity data. Data for incremental intrusion as a function of pore diameter was smoothened using a five point FFT smoothing filter to allow more effective pore size distribution analysis. Microstructural analysis was performed on a field emission scanning electron microscope (FESEM) (JEOL JSM-6700F FESEM) after the carbon

Table 1. Thermal Schedules

Oxidation		
Function	**Rate/Time**	**T (˚C)**
Ramp	5˚C/day	80-115
Ramp	115˚C/day	230
Dwell	24 hr	230
Ramp	20˚C/day	250
Dwell	5 day	250
Ramp	25˚C/hr	RT

Carbonization		
Function	**Rate/Time**	**T (˚C)**
Ramp	100˚C/hr	RT-250
Dwell	0.5hr	250
Ramp	5˚C/hr	275
Dwell	2hr	275
Ramp	5˚C/hr	325
Dwell	2hr	325
Ramp	50˚C/hr	450
Ramp	100˚C/hr	1000
Dwell	1hr	1000
Ramp	100˚C/hr	RT

Siliconization		
Function	**Rate/Time**	**T (˚C)**
Ramp	25˚C/min	RT-1000
Step	NA	1300
Dwell	30 min	1300
Step	NA	1800
Dwell	30 min	1800
Step	NA	25

samples were sectioned and their cross section ground and polished. Surface area and pore characterization was performed by nitrogen gas adsorption analysis (Coulter SA 3100) yielding adsorption isotherms and various surface areas and pore volumes determined by BET, Langmuir and t-plot theories. Actual densities of the carbons and siliconized carbons were determined by helium gas pycnometry (Micromeritics AccuPyc 1330). The SiC materials were first rid of their rough surface layer on a grinder. Since volumes smaller than that recommended were being measured (samples are recommended to take up 90% of the 10 cm^3 sample chamber) an aluminum rod was used to displace the unoccupied volume in an effort to increase accuracy of the density measurements. This was deemed effective as density measurements of small volumes of silicon (2.3318 g cm^{-3}) were very close to the actual density (2.33 g cm^{-3}) with a very small standard deviation (±0.0037). Optical images of polished cross-sections of the siliconized carbons were collected with a digital camera (Diagnostic Instruments, Inc., Insight 2 (2MP) (1600x1200), 11.2 Color Mosaic) mounted on a metallograph (Zeiss, ICM 405). Image averaging, flat-field correction, unsharp mask filtering, and image analysis were performed using a open-source java-based image analysis program (ImageJ, 1.38m).

Results and Discussion

The monolithic precursor blends are pyrolyzed leading to monolithic carbons with various microstructures. Microstructural images are presented in Figure 4. The carbon derived from pure crystalline cellulose is shown in Figure 4a and retains the initial packed cellulose particle macrostructure. Figure 4c shows the structure formed from carbonization of pure phenolic resin. The process of becoming viscous, then thermosetting then carbonizing is evident from the highly dense and glassy surface with large bubbles present from volatilized gas entrapment. The carbon microstructure formed from a precursor blend of 40 percent phenolic resin is shown in Figure 4b and shows the retention of the porous nature of the cellulose phase while exhibiting a smooth glassy surface from the phenolic phase.

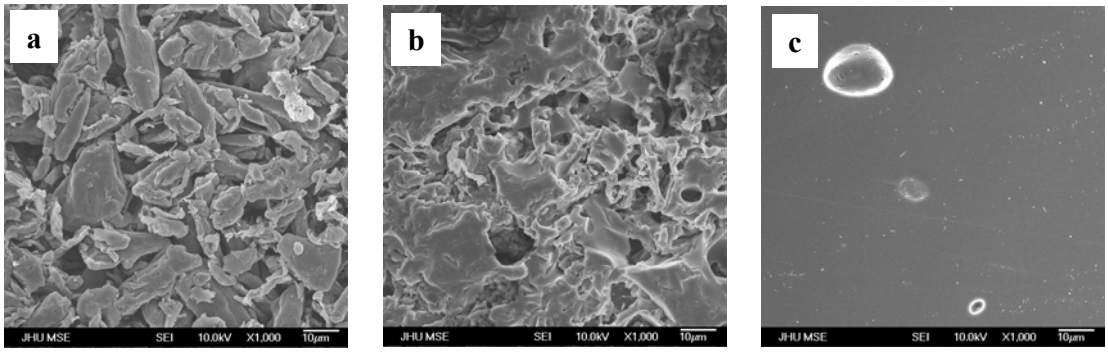

Pyrolyzation of the precursors leads to volatilization and evolution of nearly all non-carbon species in the form of CO and CO_2 in addition to a myriad of other larger molecules[2,7,8,10]. The resulting carbon yields 9 and 64 percent of the original precursor mass for crystalline cellulose and phenolic resin, respectively (See Figure 5). It was expected that the mass yields for the blends of the two precursors would follow the rule of mixtures and behave linearly between the two extremes; however, this has not occurred. During the pyrolyzation process crystalline cellulose is able to rid its structure of a large percentage of its evolved gases. As phenolic resin is blended with cellulose in small amounts this remains possible and the mass yield increases linearly initially. However, when about 50 percent phenolic resin is present in the blend the trend deviates from the initial linearity and becomes steeper. The deviation from the trend is thought to be due to the percolation of the phenolic resin phase around the cellulose phase. That is, the phenolic resin forms a completed matrix around the cellulose particles and traps some of the evolved gases being released during pyrolyzation. Thus the trend increases linearly as the precursor concentration increases from 50 percent to pure phenolic resin.

The monolithic bulk density of our blend system behaves similarly to the mass yield trends in that it shows evidence of percolation of the phenolic resin phase (See Figure 6). The bulk

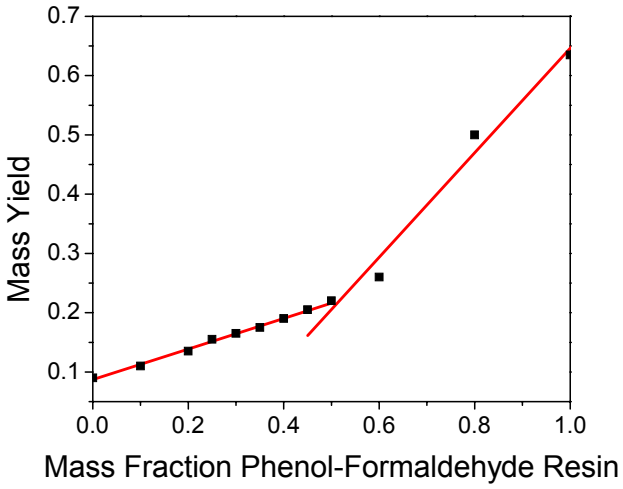

Figure 5. Mass yield of carbonized crystalline cellulose – phenolic resin precursor blends.

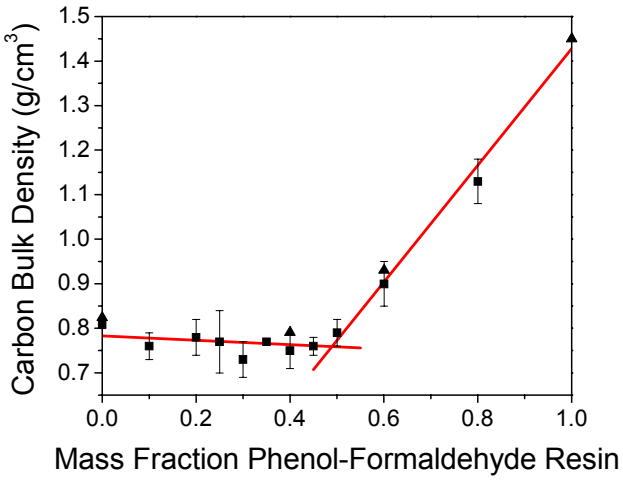

Figure 6. Bulk density of carbon monoliths made from crystalline cellulose – phenolic resin blends.

density of the pure cellulose derived carbon monolith is 0.82 g cm^{-3} and 1.45 g cm^{-3} for the phenolic resin precursor. As small amounts of phenolic resin are added to cellulose the bulk density decreases slightly and behaves linearly. The decrease in bulk density is due to the higher shrinkage of the pure cellulose precursor upon carbonization, 51% dimensional yield, in comparison to that of pure phenolic resin, 82% dimensional yield. So although the mass yield is increasing with small additions of phenolic resin the shrinkage is decreasing resulting in decreasing bulk density values. The percolation behavior of the resinous phase is again noticed at a concentration of near 50 percent of phenolic resin. This is due to the steepening of the mass yield trend shown in Figure 5. Similarly the linear trend changes to that of a steeper one as bulk density is increased from below 0.8 to 1.45 g cm^{-3}. The ideal bulk density of 0.964 g cm^{-3} is a little above the values exhibited in the first linear portion but the value for the blend with a phenolic resin concentration of 60 percent approaches the value.

The macropore distributions are represented as log differential intrusion volume vs. mean pore diameter as measured by mercury intrusion porosimetry in Figure 7. This plot emphasizes the frequency of pore diameters within a percentage range. Macropore distributions are plotted for carbons of pure cellulose, pure phenolic resin and 40 and 60 percent phenolic resin. Additional values calculated from mercury intrusion data are given in Table 2. The pure cellulose derived carbon monolith has a unimodal macropore distribution with a median pore diameter of 640 nm. The carbons derived from 40 and 60 percent phenolic resin blends had unimodal macropore distributions with median pore diameters of 1.5228 and 1.2881 µm, respectively while the pure phenolic resin is shown to have negligible macroporosity as expected.

Table 2. Mercury Intrusion Data Summary

Precursor Ratio (cellulose : resin)	Median Macropore Diameter (µm)	Average Macropore Diameter (µm)	Bulk Density (g mL^{-1})	Skeletal Density (g mL^{-1})	Macropore Volume (mL g^{-1})	Macroporosity (%)
100:0	0.6400	0.2427	0.8243	1.4307	0.5142	42.39
60:40	1.5228	0.4933	0.7910	1.3744	0.5382	42.57
40:60	1.2881	0.3410	0.9308	1.3766	0.3479	32.38
0:100	153.4947	0.2154	1.4476	1.2669	0.1182	13.02

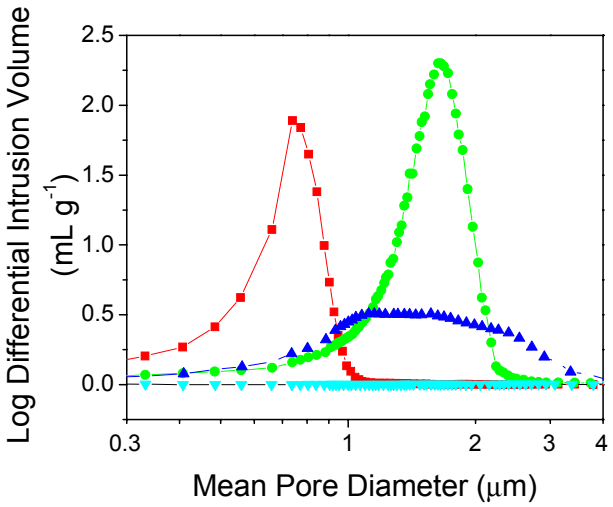

Figure 7. Pore size distribution of porous carbons created from various precursor blends. Precursor blends are represented as follows: ■ 100:0, ● 60:40, ▲ 40:60, ▼ 0:100.

Nitrogen adsorption isotherms of pure cellulose, cellulose and phenolic resin blended in a 60 to 40 ratio and pure phenolic resin are represented in Figure 8. The isotherms for cellulose and the 40 percent resin blend are quite similar in appearance and are of Type I indicating a high degree of microporosity. These materials exhibit extraordinary adsorptive capacity due to enhanced adsorption in micropores. Type I isotherms are characterized by their steep initial rise, a leveling out to a long nearly horizontal intermediate region and a final rise to saturation and bulk condensation. Adsorption takes place by micropore filling and progressively larger micropores fill in order of increasing size. Once the micropores have filled, very little adsorption takes place thereafter for there is essentially no place remaining on which adsorption can occur. Various values calculated from the nitrogen adsorption isotherm are provided in Table 3. The surface area values calculated from the Type I isotherms indicate high microporosity. For these high surface area values the Langmuir nitrogen monolayer adsorption theory for determining surface area is more appropriate giving

Langmuir surface areas, $SA_{Langmuir}$, of 654.01 and 644.75 $m^2\ g^{-1}$ for pure cellulose derived carbon and carbon derived from the blend of 40 percent phenolic resin, respectively. Additionally, t-plot theory provides micropore surface area, SA_{micro}, and meso- and macropore surface area, $SA_{t\text{-}plot}$ (mesoporosity includes pores from 2-50 nm). These values show that a substantial portion of total adsorption is occurring in micropores, however, there is a significant amount of meso- and macroporosity present in both samples. A general decrease in the various surface areas and the total pore volume, V_{ads}, is noticed as the blend is varied from pure cellulose to phenolic resin. The isotherm for pure phenolic resin derived carbon is of Type II indicative of nonporous or meso- and/or macroporous materials, although the rising nature of the linear intermediate portion in conjunction with significant t-plot surface area seems to suggest the presence of meso- and macroporosity. For a Type II isotherm BET multilayer sorption theory is preferred in calculation of surface area and yields a BET surface area, SA_{BET}, of 56.372 $m^2\ g^{-1}$ indicating significant microporosity, however, this value is much lower than that for the pure cellulose and cellulose blend derived carbons. It

Table 3. Nitrogen Adsorption Data

Precursor Ratio (cellulose : resin)	SA_{BET} ($m^2\ g^{-1}$)	$SA_{Langmuir}$ ($m^2\ g^{-1}$)	SA_{micro} ($m^2\ g^{-1}$)	$SA_{t\text{-}plot}$ ($m^2\ g^{-1}$)	V_{Ads} ($cm^3\ g^{-1}$)
100:0	528.80	654.01	484.027	44.771	0.2659
60:40	526.44	644.75	485.587	40.849	0.2545
0:100	56.372	61.901	32.307	24.065	0.0559

Table 5. Density of Siliconized Carbons

Precursor Ratio (cellulose : resin)	Density ($g\ cm^{-3}$)	Fraction of Pure SiC Density ($g\ cm^{-3}$)
65:35	2.8465	0.8840

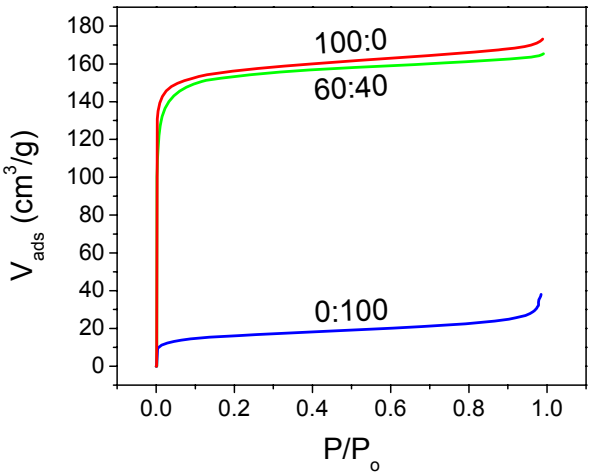

Figure 8. Nitrogen adsorption isotherms for carbons made from pure crystalline cellulose (100:0), phenolic resin (0:100) and a blend of the two (60:40).

Table 4. Carbon Actual Densities

Precursor Ratio (cellulose : resin)	Density ($g\ cm^{-3}$)	Fraction of Graphite Density ($g\ cm^{-3}$)
100:0	2.0980	0.94
60:40	2.1911	0.98
0:100	2.0271	0.91
Graphite	2.23	1.00

can thus be deduced that the majority of surface area exhibited by the carbons tested here is from the cellulosic phase and not the phenolic phase.

60:40	2.9566	0.9182
55:45	2.7585	0.8567
50:50	2.7628	0.8580
SiC	3.220	1

The actual density values for carbons derived from the same three precursors, pure cellulose, pure resin and 60 percent resin, were determined using helium gas pycnometry and are presented in Table 4. These values show that the actual density varies negatively from that of pure graphite probably due to bond length and stacking height irregularities. The decrease in actual carbon density as cellulose precursor content is increased seems to indicate decrease in graphitic character which makes sense due to the lack of easy hexagonal ring forming mechanisms of cellulose decomposition. This also suggests a higher reactivity of the cellulosic phase.

Upon siliconization at elevated temperatures various degrees of reaction are exhibited. The densities of the resulting materials are given in Table 5 for the precursor ratios that experienced significant amounts of reaction. Siliconization of the carbon derived from pure cellulose did not form a monolithic SiC whatsoever. It appears that the reactivity of this material is so high that the molten silicon easily dissolves the carbon atoms and clusters. Dissolution occurs so readily that the solute is drawn back into the silicon melt and precipitates SiC crystallites there instead of in the bulk structure of the monolith. The monolith is essentially dissolved away. The extremely high reactivity of the cellulosic carbon phase is represented by their high nitrogen adsorption capacity. The high surface areas of this phase indicates a very high concentration of active sites and a large network of nanometer scale tunnels for the silicon atoms to reach them. The low actual density value also supports this as a deviation from graphitic character suggests a high concentration of active sites.

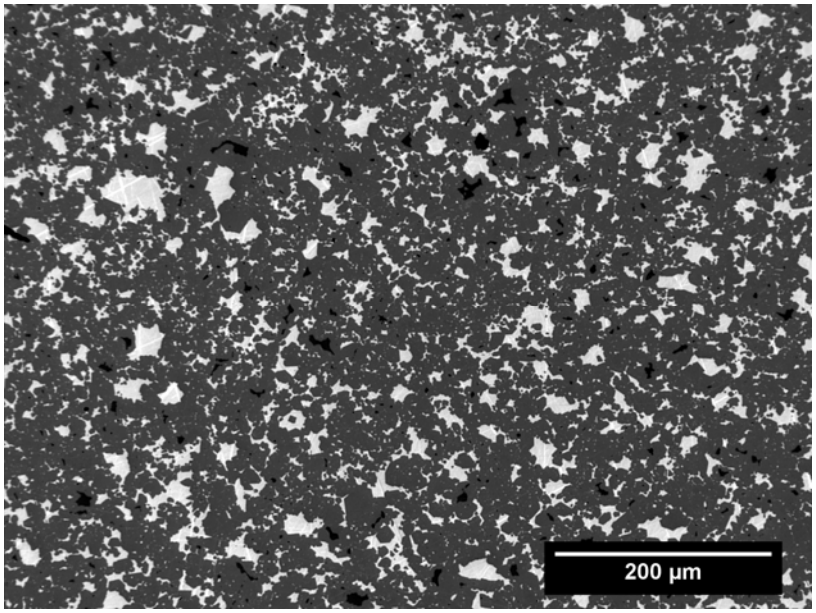

Figure 9. Optical micrograph of polished cross-section of siliconized carbon. Black regions are C, gray are SiC, and white are Si.

Conversely, the low reactivity of the carbon phase derived from phenolic resin is evident in its actual density that approaches that of graphite and it's much lower microporosity and surface area. The actual density of pure phenolic resin decreases due to the presence of closed microporosity. But the increase in graphitic character is shown by the increase in density for the blend containing 40 percent resin as compared to that of pure cellulose. As a result of the lower reactivity the reaction can only occur at the carbon surface creating a SiC layer maximum thickness of 10 µm. As the phenolic resin content is reduced the gains of the highly reactive cellulose phase can be taken advantage of, however, for the case of 60 percent resin macroporosity prevents effective siliconization. Although the ideal bulk density is approached and the median pore diameter is above 1 µm the average pore diameter is too low, that is, the amount of

pores that occur at a diameter greater than 1 μm is too low to allow effective siliconization and as a result, pore choking was observed.

The precursor ratios between 65:35 and 50:50 yielded successful bulk siliconizations. In these materials reaction occurred throughout the entire sample cross-sections. It is believed that this is due to the reactivity being sufficient for effective siliconization without being too high as is the case for pure cellulose precursor. The lower reactivity of the phenolic based carbon phase maintains structural rigidity of the bulk structure. Additionally, the median pore diameters are greater than 1 μm and the pore size distributions are relatively narrow thus preventing pore choking. The porous carbon derived from the precursor blend containing 40 percent phenolic resin yielded the highest density of 2.9566 g cm^{-3} which is over 91 percent of pure SiC density. An optical image of this material is shown in Figure 9 and shows no residual porosity and over 80 volume percent SiC comprising the microstructure with the remaining portions being unreacted silicon and carbon.

Conclusions

The bulk density, macroporosity and reactivity of the carbon substrate are paramount in determining the effectiveness of bulk silicon infiltration and SiC formation. We have demonstrated that by varying precursor composition one can tune these properties. By blending crystalline cellulose and phenolic resin as precursors to monolithic carbon substrates we successfully controlled the carbon bulk density, macroporosity and reactivity. The bulk density was varied between 0.75 and 1.45 g cm^{-3}. We successfully tuned macroporosity yielding narrow unimodal macropore size distributions above 1 um thus eliminating pore choking and maximizing fluid velocity into the porous carbon. Additionally, we varied carbon reactivity by creating a highly reactive cellulosic phase tempered by the rigid and lower reactivity resinous phase. These efforts led to a fully-dense SiC material with a density over 91% that of pure SiC and a volume fraction of over 80% SiC.

Acknowledgement

The authors would like to acknowledge the sponsorship and funding from the Department of Energy (DOE) under the Nuclear Energy Research Initiative (NERI), 2.2 Next Generation Nuclear Plant (NGNP), 2.2.2 Materials Related to the NGNP Project.

References

1. D.R. Behrendt and M. Singh. "Effect of carbon preform pore volume and infiltrants on the composition of reaction-formed silicon carbide materials ," J. Mater. Synth. Process., **2,** 117-123 (1994).

2. C.E. Byrne and D.C. Nagle. "Carbonized wood monoliths - Characterization," Carbon, **35,** 267-73 (1997).

3. C.E. Byrne and D.C. Nagle. "Carbonization of wood for advanced materials applications," Carbon, **35,** 259-66 (1997).

4. C.E. Byrne and D.C. Nagle. "Cellulose derived composites - A new method for materials processing," Materials Research Innovations, **1,** 137-44 (1997).

5. Y.M. Chiang, R.P. Messner, C.D. Terwilliger and D.R. Behrendt. "Reaction-Formed Silicon-Carbide," Materials Science and Engineering A-Structural Materials Properties Microstructure and Processing, **144,** 63-74 (1991).

6. A. Favre, H. Fuzellier and J. Suptil. "An original way to investigate the siliconizing of carbon materials," Ceram. Int., **29,** 235-43 (2003).

7. A.K. Kercher and D.C. Nagle. "Monolithic activated carbon sheets from carbonized medium-density fiberboard," Carbon, **41,** 3-13 (2003).

8. A.K. Kercher and D.C. Nagle. "Evaluation of carbonized medium-density fiberboard for electrical applications," Carbon, **40,** 1321-30 (2002).

9. R.P. Messner and Y.M. Chiang. "Liquid-Phase Reaction-Bonding of Silicon-Carbide using Alloyed Silicon Molybdenum Melts," J Am Ceram Soc, **73,** 1193-200 (1990).

10. F. Shafizadeh, "The Chemistry of Pyrolysis and Combustion," Advances in Chemistry Series, 491-529 (1984).

11. Y.X. Wang, S.H. Tan and D.L. Jiang. "The effect of porous carbon preform and the infiltration process on the properties of reaction-formed SiC," Carbon, **42,** 1833-9 (2004).

12. H. Zhou and R.N. Singh. "Kinetics Model for the Growth of Silicon-Carbide by the Reaction of Liquid Silicon with Carbon," J Am Ceram Soc, **78,** 2456-62 (1995).